INSTITUTE OF PHYSICS PUBLISHING MEASUREMENT SCIENCE AND TECHNOLOGY

Meas. Sci. Technol. **16** (2005) 1299–1304 doi:10.1088/0957-0233/16/6/009

Fibre optic distributed temperature sensor with an integrated background correction function

P R Stoddart[1], P J Cadusch[1], J B Pearce[1], D Vukovic[2], C R Nagarajah[2] and D J Booth[1]

[1] Centre for Atom Optics and Ultrafast Spectroscopy, Faculty of Engineering and Industrial Science, Swinburne University of Technology, Mail H38, PO Box 218, Hawthorn, VIC 3122, Australia

[2] Industrial Research Institute Swinburne, Swinburne University of Technology, Mail H31, PO Box 218, Hawthorn, VIC 3122, Australia

E-mail: pstoddart@swin.edu.au

Received 28 January 2005, in final form 24 March 2005
Published 4 May 2005
Online at stacks.iop.org/MST/16/1299

Abstract

Raman scattering in optical fibres provides a means of measuring continuous temperature distributions over extended distances. However, in many applications it has been found that the background transmission properties of the optical fibre either change after deployment of the fibre or vary over time due to ageing effects. Changes in the fibre transmission can be distinguished from thermal effects by measuring the Rayleigh backscatter, which is relatively insensitive to temperature. The combined use of Raman and Rayleigh data is discussed here in the context of a particularly simple and cost-effective sensor design, where a single, fixed optical filter and a single light source are used for both measurement modes. The Rayleigh backscatter measurement allows the accurate correction of background transmission changes in a probe arrangement that includes several splices between different fibres with different attenuations. In this way, the temperature in a 290 °C test region is accurately recovered from the anti-Stokes Raman signal. However, preliminary measurements of the fibre attenuation as a function of temperature and exposure to an accelerated ageing environment show that these two effects will be difficult to separate in practice. Therefore it remains challenging to perform accurate, unambiguous background corrections in situations where high-temperature ageing occurs.

Keywords: optical fibre sensors, Raman scattering, distributed temperature measurements

1. Introduction

A distributed temperature sensor (DTS) is able to provide a temperature reading as a continuous function of position along the optical fibre sensor element. A number of DTS implementations have been proposed over the years [1–4]. These are primarily based on intrinsic sensing mechanisms, i.e., the fibre provides the sensing medium. To date, devices based on spontaneous Raman scattering in solid core optical fibres [5] have perhaps been the most widely applied in industry and have now reached a relatively advanced level of sophistication [6]. These systems typically use the more temperature-sensitive anti-Stokes Raman band to measure the temperature distribution. The DTS system described in this paper (Sentor 101, Tyree Optech) is based on the photon counting detection of anti-Stokes Raman scattering generated in a multi-mode optical fibre by a low power 780 nm laser diode.

Although DTS systems have had some commercial success, particularly in fire detection and oil well monitoring applications, it is recognized that the technology will have to be more price competitive with electrical sensors before more widespread market acceptance can be achieved. The accuracy of the measurements also remains an issue, particularly in the more demanding applications. Deployment of the optical fibre in the field generally leads to strains and kinks that can modify the local attenuation of the fibre. These background effects can be reduced by referencing the anti-Stokes signal to another less temperature sensitive signal, such as the Stokes Raman band [5], or the Rayleigh backscatter [7].

The backscattered signal is dominated by the exponential dependence of the optical transmission through the optical fibre. This dependence is described by the attenuation coefficient α, which is typically reported in units of dB km^{-1}. In the present DTS, the temperature-dependent anti-Stokes signal can be described by

$$I_{\mathrm{as}}(z, T) = A_{\mathrm{as}}(T) f(z) \, \mathrm{e}^{-\alpha_{\mathrm{DTS}} z} + C,$$

where C is a constant background dark count level and $\alpha_{\mathrm{DTS}} = \alpha_0 + \alpha_{\mathrm{as}}$ which accounts for attenuation of the outgoing laser wavelength and the backscattered anti-Stokes wavelength, respectively. $A_{\mathrm{as}}(T)$ is the temperature-dependent anti-Stokes Raman scattering cross section, while $f(z)$ describes all other transmission-related background features such as attenuation variations, splices, connectors, strain and so forth. It is assumed that these factors are both wavelength and temperature independent to a first approximation.

The system incorporates an optical time-domain reflectometry (OTDR) functionality that generates a Rayleigh backscatter trace for fibre background corrections. This arrangement is cost competitive as both the DTS and OTDR modes of operation have a common, fixed optical filter and a single light source and detector. The OTDR measurement is only weakly temperature dependent, as the Rayleigh scattering has a relative temperature sensitivity of approximately 0.005% $^{\circ}$C^{-1} in solid core fibres, compared to a sensitivity of 0.8% $^{\circ}$C^{-1} for the anti-Stokes scattering [1]. The OTDR measurement also has a slightly different attenuation $\alpha_{\mathrm{OTDR}} = 2\alpha_{\mathrm{as}}$, because the scattering is now elastic (outgoing and backscattered wavelengths are the same). This is achieved by running the laser diode below the laser threshold, so that the broadband of spontaneously emitted light overlaps with the filter window at about 750 nm. The OTDR signal can therefore be approximated as

$$I_R(z) = A_R f(z) \, \mathrm{e}^{-\alpha_{\mathrm{OTDR}} z} + D,$$

where we assume that the function $f(z)$ is still valid, despite the change in the outgoing wavelength. For practical application of this technique, it is desirable to use the OTDR measurement to remove all of the range-dependent factors and in particular the arbitrary background features incorporated into $f(z)$. This can be done by taking the ratio of the background corrected DTS and OTDR measurements

$$\begin{aligned} I'(z, T) &= \frac{I_{\mathrm{as}} - C}{I_R - D} = A'(T) \, \mathrm{e}^{-(\alpha_{\mathrm{DTS}} - \alpha_{\mathrm{OTDR}}) z} \\ &= A'(T) \, \mathrm{e}^{-(\alpha_0 - \alpha_{\mathrm{as}}) z}, \end{aligned} \tag{1}$$

where $A'(T) = A_{\mathrm{as}}(T)/A_R$. Clearly, the attenuation-related exponential dependence can be reduced in this way, but not totally removed.

In contrast, if the ratio between anti-Stokes and Stokes intensities was taken, the remaining exponential dependence would be $\mathrm{e}^{-(\alpha_{\mathrm{as}} - \alpha_s) z}$. The residual exponential dependence is therefore more severe, because

$$|\alpha_{\mathrm{as}} - \alpha_s| \approx 2|\alpha_0 - \alpha_{\mathrm{as}}|.$$

All of the attenuation coefficients can, in principle, be obtained by subjecting the fibre to a known temperature distribution. However, each of the attenuation factors has a slightly different temperature dependence. This has led to the use of more elaborate signal-processing methods, where the attenuation value is iteratively corrected for the calculated temperature at each point [8]. Alternatively, the fibre may be measured from both ends [9], with an attendant loss of flexibility and overall range. In this paper, we also show that the attenuation can be adversely affected by fibre degradation, as might occur in the hot and humid environment of an oil well. These issues suggest a potential advantage of the present system, in that the smaller residual range dependence may be more easily corrected.

Corrections of background transmission variations by the referencing method may also be affected by a difference in sensitivity to modal effects at bends or connectors at the two different wavelengths. This is apparent from the wavelength dependence of the normalized frequency

$$V = \frac{2\pi a}{\lambda} \mathrm{NA}$$

where NA is the numerical aperture of the fibre. This leads to a different number of allowed modes for propagation at the laser and filter wavelengths. For large V, the number of modes is given by

$$M \approx V^2/2 \propto \frac{1}{\lambda^2},$$

which suggests that about 8% more modes can propagate at the wavelength of the filter (750 nm) than at the wavelength of the source (780 nm). Once again, this effect will be more severe for the more widely separated wavelengths that apply in the anti-Stokes : Stokes ratio method.

More recently, a DTS system has been implemented in single-mode fibre [6]. It has been claimed that all of the transmission losses in single-mode DTS systems can be accurately referenced, thereby eliminating the need for double-ended measurements [1]. Single-mode operation also allows access to high-quality telecommunications components in the low-loss 1550 nm transmission window. However, photon counting is not yet viable at these wavelengths and the Raman signal level is reduced, which implies a need for photodiode-based detectors and relatively expensive, high-power laser sources. The detector sensitivity is reduced at these wavelengths and stringent temperature control is required to ensure stability. These factors suggest that single-mode systems are unlikely to deliver the desired cost reductions.

This paper examines the efficacy of the anti-Stokes : Rayleigh referencing technique described above. Preliminary results for the degradation in the transmission of the optical fibre under simulated down-well conditions are also presented. The implications of this degradation are discussed in the context of background corrections performed via the referencing technique.

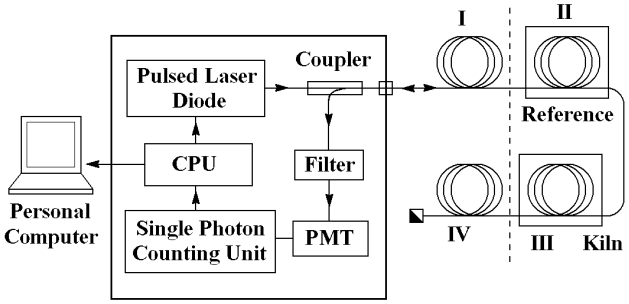

Figure 1. Schematic diagram of the distributed temperature sensor system, showing the arrangement of optical fibres used in the fibre ageing experiment.

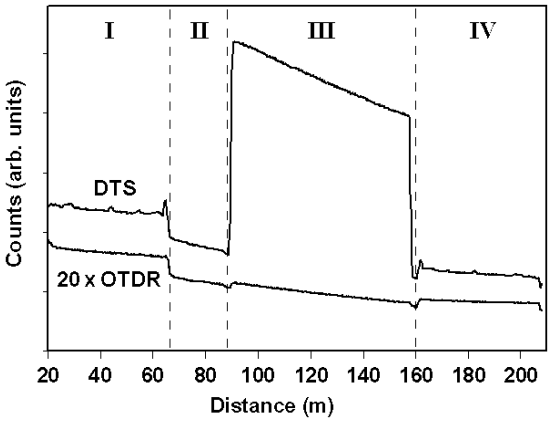

Figure 2. Anti-Stokes (DTS) and Rayleigh (OTDR) signals obtained for an arrangement of two different fibres in four different regions (I, II, III, IV), as described in the text.

2. Experimental details

An experimental arrangement was devised to evaluate the effects of accelerated ageing on a standard high-temperature fibre. At the same time, the set-up served to generate a reasonably complex data set to test the performance of the anti-Stokes : Rayleigh reference method. The arrangement is illustrated in figure 1. The laser diode has a peak power output of about 70 mW, with a pulse length of less than 10 ns. The interference filter has a 10 nm passband centred on 750 nm and an average optical density of 6 outside the passband. The arrival time of the backscattered photons is resolved with 2 ns precision by a proprietary multichannel scaler and the photon counts accumulated over many laser pulses are stored in bins corresponding to this period. A standard multi-mode optical fibre cable was used to connect the DTS unit through region I to a remote high-temperature fibre (OFS, carbon/polyimide coated). This fibre consisted of a 20 m section that was placed in a thermally insulated container (region II) and used as a room-temperature reference. The reference temperature was measured by means of a thermistor. The reference section was in turn spliced to a longer section of high-temperature fibre that was placed in an oil bath in a kiln (region III). The far end of the fibre in region III was spliced to a second multi-mode cable that retraced the path from the kiln to the DTS unit (region IV). Note that region IV should provide an almost identical thermal environment to region I, but in reverse.

The kiln was heated to a nominal temperature of 290 °C and a sequence of DTS and OTDR measurements was performed on a daily basis over a three-day period. On the third day, a silicone-based oil was injected into the oil vessel in order to accelerate the ageing. Thereafter, measurements were performed approximately on a two-hourly basis. Sample results from day 1 are shown in figure 2, together with the approximate positions of the various regions. The DTS signal shows a significant increase in amplitude in the hot zone (region III). A number of other minor temperature features can also be seen in region I, together with splice losses that are particularly apparent at about 66 m and 88 m. These features will be discussed in further detail below.

The OTDR signal is magnified here to appear on the same scale as the DTS signal. The OTDR data were collected over a period of 8 h, compared to 10 min for the DTS. Both data sets have been smoothed to yield an effective spatial resolution of 1.0 m. The small OTDR count rate reflects the modest overlap between the spontaneous emission of the laser diode and the filter window used in this configuration. However, the background features probed by the OTDR mode are normally only slowly changing (e.g., in response to fibre ageing) and can therefore be averaged over relatively long periods. In most applications, the inconvenience of lengthy OTDR averaging will be easily justified by the cost advantage of the integrated OTDR mode.

In a separate experiment, a new section of the high temperature fibre was coiled on a steel plate in a conventional temperature-controlled furnace. DTS and OTDR measurements were performed from room temperature up to about 300 °C so that the temperature dependence of the two attenuation coefficients could be studied.

3. Results and discussion

The fibre arrangement used in these tests has several features that would normally render the results difficult to interpret. These include the three splices, as well as an increased attenuation in region II, which has been attributed to bending losses in the coiled reference section. Region III has also been exposed to a chemical environment that has resulted in accelerated ageing of the fibre and hence an increased attenuation. Therefore, the data shown in figure 2 provide a reasonably challenging test of the anti-Stokes : Rayleigh reference technique.

An automated background correction procedure would typically involve the following steps:

(a) Identification of step discontinuities, such as might occur at connectors, splices and microbends.
(b) Use the dataset between each step to obtain an estimate of α_{OTDR}.
(c) Use α_{OTDR} to predict α_{DTS}, based on a comprehensive characterisation of the particular fibre being used and assuming some convenient initial temperature distribution over the range.
(d) Calculate $I'(z, T)$ as shown in equation (1) and multiply through by $\mathrm{e}^{(\alpha_{\mathrm{DTS}}-\alpha_{\mathrm{OTDRs}})z}$ to remove the residual exponential dependence.
(e) Derive the temperature distribution in the normal way (see below);

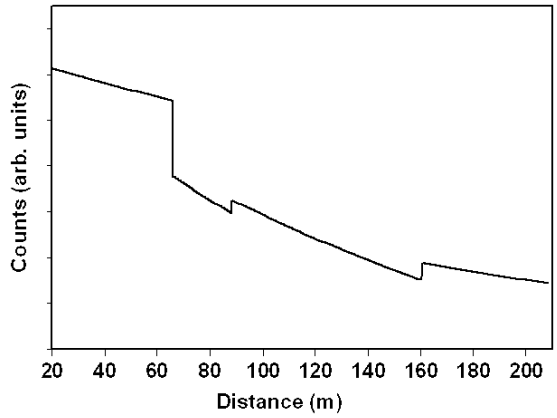

Figure 3. Identification of edges in the OTDR data set. Comparison of the exponential fits with the raw data suggests that each section has a reasonably well-defined attenuation. The raw data are not shown here for clarity.

Table 1. DTS and OTDR attenuation factors calculated for the different regions of the dataset in figure 2.

Region	α_{DTS} (dB km^{-1})	α_{OTDR} (dB km^{-1})	$\alpha_{\mathrm{DTS}} - \alpha_{\mathrm{OTDR}}$ (dB km^{-1})
I	6.4	8.2	−1.8
II	23.7	27.1	−3.4
III	18.3	21.9	−3.6
IV	8.4	9.9	−1.5

(f) Iterate steps (c) to (e), using the updated estimate for the temperature distribution to improve the prediction of α_{DTS} based on α_{OTDR}, until the desired accuracy is reached.

The relationship between the attenuation factors α_{DTS} and α_{OTDR} was not known *a priori* for the two different optical fibres used to obtain the data shown in figure 2. Therefore they were calculated from representative sections of the DTS and OTDR data set in each of the four regions. This approach will only be valid in cases where the temperature is known to be relatively constant in a region. The regions themselves were defined by passing an edge detector over the full OTDR data set of figure 2. The exact regions are shown in figure 3, together with the respective exponential curves found from a least squares fitting procedure. The various attenuation factors are shown in table 1, together with the values estimated from the DTS data. Note that the attenuation factors are based on the exponential dependence of the transmission function as defined in section 1. These values have been multiplied by a factor of $10 \log \mathrm{e} = 4.343$ in order to convert the attenuation into the commonly quoted decibels per kilometre.

Based on the data shown in table 1, the ratio of DTS to OTDR data was corrected for the residual exponential dependence shown in equation (1). The DTS:OTDR ratio was found by simply dividing the two data sets through on a point-by-point basis. The background corrected data were then converted to temperature by solving the equation for $A'(T)$. This calculation requires a factor that relates to the anti-Stokes scattering cross section, which is proportional to the equilibrium phonon population given by the Planck distribution function [10]. The factor is typically obtained from a reference region of known temperature. For the data set

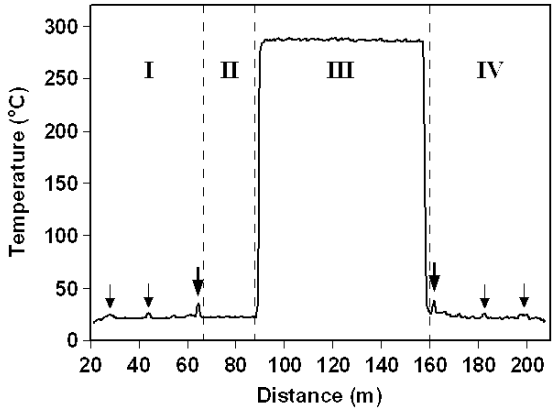

Figure 4. The 290 °C test region is recovered after the background corrected data are converted to temperature. The features indicated by the bold arrows are caused by the standard fibre passing close by the warm external surface of the kiln. The light arrows point to smaller peaks that are due to the fibres passing beneath warm air conditioning ducts.

discussed here, a conversion factor was obtained from region II and this was found to give sensible results for the high-temperature fibre in regions II and III. However, a slightly different conversion factor was required for the standard fibres in order to match the room temperature levels in regions I and IV. This can be attributed to slightly different anti-Stokes Raman scattering cross sections for the two different fibre types.

The expected temperature dependence is reproduced satisfactorily by this analysis, as shown in figure 4. The minor features indicated by the light arrows are due to the fibre passing under warm air conditioning ducts, while the peaks indicated by the bold arrows arise from the fibre passing close to the hot outer casing of the kiln. These features are reproduced in reverse order on the return path. The average temperature in the kiln is found to be 287 °C, which agrees reasonably well with the 290 ± 7 °C set point of the kiln. The standard deviation in region III is 1.2 °C, which corresponds to a standard error of 0.6 °C over 1 m (i.e., five measurement points). Careful calibration testing of the DTS measurement function over the range 0–100 °C has shown that the temperature calculation algorithm overestimates the slope of the relationship between calculated and true temperatures by about 3%. This inaccuracy in the temperature conversion algorithm is consistent with small variations in anti-Stokes scattering intensity across the window of the bandpass filter. The relatively good agreement of the temperature found here suggests that the small temperature dependence of the OTDR measurement serves to compensate to some extent for the effects of this calibration error. This is reasonable, as an increase in OTDR amplitude would tend to reduce the indicated temperature. Further measurements would be required to quantify this effect.

The background correction implemented here has not accounted for the mode settling effects immediately after the connector at 20 m. The results also suggest that the return path immediately after the spike at 163 m is about 2–4 °C warmer than the equivalent section in region I. Given the collocation of the fibres in regions I and IV, it seems unlikely that this feature has a thermal origin. The 'warming' effect decreases

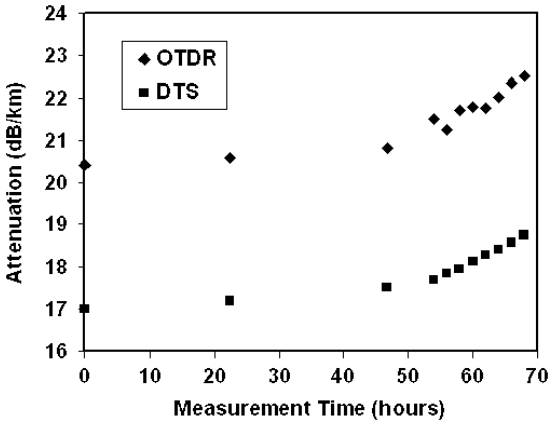

Figure 5. DTS and OTDR attenuation factors in the high-temperature fibre, as a function of time under simulated ageing conditions. Silicone oil was injected after approximately 50 h in order to accelerate the ageing process.

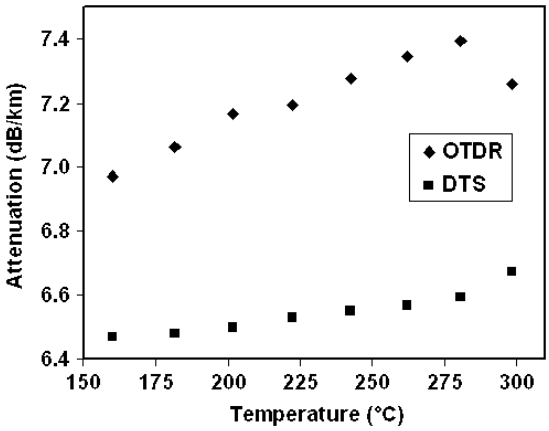

Figure 6. DTS and OTDR attenuation factors as a function of temperature in high-temperature fibre as received.

rapidly over an interval of about 10 m from the splice and might therefore be associated with mode settling effects. However, these defects are relatively minor and the overall performance is quite satisfactory.

From the above discussion, it is clear that the main obstacle to automating the background correction lies in the prediction of α_{DTS} based on α_{OTDR}, as discussed in step (c) of the above procedure. The attenuation is material dependent, so the correction factor $e^{(\alpha_{\mathrm{DTS}}-\alpha_{\mathrm{OTDR}_S})z}$ must be determined for each type of fibre that is of interest. In addition, the attenuation factors themselves have some temperature dependence, which is mainly due to the small temperature dependence of the Rayleigh scattering. If the variation in attenuation with temperature is known, then an iterative approach can be used to correct the attenuation factors after each calculation of the temperature.

The optical properties of the materials are also likely to change with time. For example, germanosilicate core fibres display increased losses at short wavelengths after exposure to H_2 at 150–250 °C [11, 12], while ambient molecular water is known to efficiently drive the growth of micro-cracks on the surface of glass fibres under stress [13]. Although the precise degradation mechanisms are not yet fully understood, the darkening of optical fibre is particularly severe for down-well applications in the oil and gas industry, where fibre is exposed to H- and OH-rich compounds at elevated temperatures. Therefore a complete characterization of α_{OTDR} and α_{DTS} for a particular fibre type must take into account all of these factors. It is not yet clear whether this characterization can be performed to the required level of confidence for all materials of interest.

Some preliminary results comparing α_{OTDR} and α_{DTS} are shown in figures 5 and 6 for the OFS high-temperature optical fibre. Figure 5 shows the change in attenuation during accelerated ageing of the fibre in an oil bath at approximately 290°C. The fibre had already experienced some ageing before the measurement sequence was performed. The ageing process was accelerated by the injection of a silicone oil some 50 hours after the first measurement was performed. The temperature dependence of the attenuation in a length of virgin fibre is shown in figure 6. As expected, the OTDR attenuation factors show somewhat higher scatter for the 1 h OTDR measurements used here. The accuracy of the results could again be improved by accumulating an average OTDR trace over an extended period. On the other hand, the DTS attenuation can be obtained reasonably accurately from a 10 min measurement. Therefore, the sudden change in the attenuation factors at 300 °C is probably reliable and might be associated with degradation or softening of the polyimide coating. The coating is only rated for operation up to 300 °C.

The average attenuation ratio (α_{OTDR}:α_{DTS}) varies from 1.20 to 1.10 for the data in figures 5 and 6 respectively. Although this variation is relatively large, the ratio is reasonably consistent for each data set. It is also interesting to note that this ratio is limited to a minimum value of 1.08 by the $1/\lambda^4$ dependence of Rayleigh scattering in a fibre with negligible absorption. Therefore the ratio is expected to increase as a function of the absorption introduced by the ageing processes. A more comprehensive study will be required to measure all relevant performance conditions and to understand the reproducibility of these results over the full lifetime of different fibre batches.

4. Conclusion

The results shown here indicate that a simple DTS system based on a single, fixed optical filter and a single photon-counting detector can successfully be used to perform accurate temperature measurements in relatively complex arrangements of optical fibre. The success of the measurements is largely due to the ability to perform a background correction, based on an OTDR measurement of the transmission through the optical fibre cables. This system is able to perform both DTS and OTDR measurements with a single light source, which ensures that the system is highly cost-competitive. This arrangement has been shown to provide a precision of about 1–2 °C over distances of 2–3 km for measurement times of 600 s and spatial averaging over 1 m. The intrinsic instrumental profile width is approximately 0.6 m.

For many harsh industrial environments, the long-term accuracy of DTS measurements is likely to depend on the performance of corrections for changes in the transmission

properties of the optical fibre probe. In oil and gas wells, optical fibres exposed to high temperatures and hydrogen-rich environments for extended periods are known to darken over time. These ageing effects have a complex dependence on the optical materials, operating wavelength, exposure time and temperature over the length of the fibre. In addition, the attenuation itself has a significant temperature dependence, as shown in figure 6. This is partly due to the relatively small but non-zero temperature dependence of the Rayleigh scattering. As a result, the optical fibre transmission properties will be difficult to parametrize in a way that will allow accurate background corrections to be applied unambiguously for all fibre types of interest. In particular, the measurement of α_{OTDR} in a given section of fibre might not allow α_{DTS} to be predicted with sufficient accuracy.

At this stage, it appears that little is known about the chemical processes that lead to increased absorption in the down-well environment. Further work in this regard might facilitate the development of optical fibres with improved resistance to chemical attack [12].

Acknowledgments

The authors thank the CRC for Intelligent Manufacturing Systems and Technologies for financial support; Ian K Hook and Peter J Seebacher of Tyree Optech P/L assembled the prototype system used in this study; Kirby Jabusch and Colin Bussiere of Promore Division, Core Laboratories Canada Ltd assisted in setting up and performing the accelerated ageing experiments.

References

[1] Hartog A H 2000 Distributed fiber-optic sensors: principles and applications *Optical Fibre Sensor Technology* ed K T V Grattan and B T Meggitt (Dordrecht: Kluwer) pp 241–301

[2] Dakin J P 1989 Distributed optical fiber sensor systems *Optical Fiber Sensors: Systems and Applications* vol 2 ed B Culshaw and J Dakin (Boston, MA: Artech House) pp 575–97

[3] Horiguchi T, Rogers A, Michie W C, Stewart G and Culshaw B 1997 Distributed sensors: recent developments *Optical Fiber Sensors: Applications, Analysis, and Future Trends,* vol 4 ed J Dakin and B Culshaw (Boston, MA: Artech House) pp 309–68

[4] Alahbabi M N, Lawrence N P, Cho Y T and Newson T P 2004 High spatial resolution microwave detection system for Brillouin-based distributed temperature and strain sensors *Meas. Sci. Technol.* **15** 1539–43

[5] Dakin J P, Pratt D J, Bibby G W and Ross J N 1985 Distributed optical fibre Raman temperature sensor using a semiconductor light source and detector *Electron. Lett.* **21** 569–70

[6] Hartog A H 1995 Distributed fiber-optic temperature sensors: technology and applications in the power industry *Power Eng. J.* **9** 114–20

[7] Farries M C 1987 A temperature sensor *UK Patent Application* GB 2183821 A

[8] Tanabe Y, Takada A, Ikawa K and Bando N 1989 An improvement of the accuracy in the distributed fiber temperature measurement using Raman backscattering *Optical Fibre Sensors (Springer Proc. in Phys.* vol 44) ed H J Arditty, J P Dakin and R Th Kersten (Berlin: Springer) pp 537–43

[9] Hartog A H, Leach A P and Gold M P 1985 Distributed temperature sensing in solid-core fibres *Electron. Lett.* **21** 1061–63

[10] Hart T R, Aggarwal R L and Lax B 1970 Temperature dependence of Raman scattering in silicon *Phys. Rev.* B **1** 638–42

[11] Atkins R M and Lemaire P J 1992 Effects of elevated temperature hydrogen exposure on short-wavelength optical losses and defect concentrations in germanosilicate optical fibers *J. Appl. Phys.* **72** 344–48

[12] Yamamoto Y, Sasaki T, Tari T, Hirano M, Ishikawa S, Onishi M, Sasaoka E and Chigusa Y 2004 Water-free pure-silica-core fibre and its stability against hydrogen ageing *Electron. Lett.* **40** 1401–3

[13] Gy R 2003 Stress corrosion of silicate glass: a review *J. Non-Cryst. Solids* **316** 1–11